The Layered Borates $Ba_3M(BO_3)_3$ (M = Dy, Ho, Y, Er, Tm, Yb, Lu, and Sc)

James R. Cox, Douglas A. Keszler,* and Jinfan Huang

Department of Chemistry and Center for Advanced Materials Research, Oregon State University, Gilbert Hall 153, Corvallis, Oregon 97331-4003

Received April 20, 1994. Revised Manuscript Received August 29, 1994[⊗]

A new family of borates of formulation $Ba_3M(BO_3)_3$ (M = Dy, Ho, Y, Er, Tm, Yb, Lu, and Sc) has been synthesized. The structure of the Sc derivative has been determined by single-crystal X-ray methods. It crystallizes in space group $P6_3cm$ with six formula units in a cell of dimensions a = 9.227(2), c = 17.135(3) Å, and V = 1227.2(5) Å^3. The structure contains layers of triangular planar BO_3 groups that are interleaved by 9-coordinate Ba atoms and 6-coordinate Sc atoms. Analysis of powder X-ray diffraction data indicates that the analogues containing the M atoms listed above are isostructural to the Sc derivative. Analysis of photoluminescence and powder X-ray data for the solid solution $Ba_3Y_{1-x}Eu_x(BO_3)_3$ reveals the maximum size of the M atom that can be incorporated into the structure. Thermal and melting characteristics for each of the M derivatives are also described.

Introduction

This paper is the second in a series of reports on new borates having the formula $A_3M(BO_3)_3$. In this contribution we present results on the compounds having A = Ba and M = Dy, Ho, Y, Er, Tm, Yb, Lu, and Sc. These materials adopt a layered-type structure that is different from the atomic arrangement found for the compound $Sr_3Sc(BO_3)_3$ described in the previous paper.[1] The structure is examined in detail by considering the compound $Ba_3Sc(BO_3)_3$. The crystal chemistry of the family has been partially developed by establishing its structure field of existence and examining the solid solution $Ba_3Y_{1-x}Eu_x(BO_3)_3$.

Much of this work is an outgrowth of our study of phase equilibria in the system $BaO-Sc_2O_3-B_2O_3$[2] and our search for new materials that will exhibit efficient Cr^{3+} luminescence and lasing.

Experimental Section

Synthesis, Crystal Growth, and X-ray Work. Powder samples were prepared by high-temperature solid-state techniques. Stoichiometric mixtures of nitrate and oxide reagents [$Ba(NO_3)_2$ (AESAR 99.9%); B_2O_3 (AESAR 99.98%); Sc_2O_3 (Boulder Scientific 99.9%); Dy_2O_3, Y_2O_3, Yb_2O_3, and Tm_2O_3 (AESAR 99.9%); Ho_2O_3 (Cerac 99.9%); Lu_2O_3 (Rare Earth Products 99.9%)] were ground together under hexane. They were then heated in alumina crucibles for 1 h at 600 °C to decompose the nitrate. The mixtures were again ground, placed in Pt crucibles, and heated for 30 min at 700 °C, 30 min at 800 °C, and then 12–24 h at an appropriate temperature to achieve sintering; these final temperatures ranged from 850 to 1025 °C.

X-ray powder data were collected by using an automated Philips diffractometer interfaced to a PC via a MetraByte DASH 8 data acquisition board. Each derivative was found to be isostructural to the compound $Ba_3Sc(BO_3)_3$; no peaks attributable to impurity phases were identified in the powder patterns. As a result, reflection indexes were assigned by comparison to the cell of the Sc compound. Peak positions of 10–13 reflections in the region 28 < 2θ < 60° were corrected by using NIST Si standard 640b. Unit-cell parameters were optimized by least-squares refinement with the computer program POLSQ.

Single crystals of $Ba_3Sc(BO_3)_3$ were grown by heating the compound above its melting point in a Pt crucible followed by cooling the melt at 6 °C/h from 1300 to 1000 °C and then to room temperature over 8 h. A clear, crystalline block of approximate dimensions 0.3 × 0.2 × 0.2 mm was obtained from the resulting solid and mounted on a glass fiber for data collection. Unit-cell parameters were refined from 17 reflections in the range 30 < 2θ < 43° that were automatically centered on a Rigaku AFC6R X-ray diffractometer. The Laue symmetry was found to be $6/mmm$. Data were collected at a temperature of 23 °C for indices 0 < h < 14, 0 < k < 14, and 0 < l < 27 by using the ω-scan technique to a maximum 2θ value of 80.0°. Scans of (1.55 + 0.30 tan θ)° were made at a speed of 16.0°/min in ω. The intensities of three representative reflections that were measured after every 250 data remained constant throughout the collection, indicating crystal and electronic stability. A total of 1648 reflections were collected with 1236 observations having $F_o^2 > 3\sigma(F_o2)$.

Calculations were performed on a μVAX II computer by using programs from the TEXSAN crystallographic software package.[3] The systematically absent reflections $00l$, $l = 2n + 1$, and the successful refinement of the structure indicate the correct space group is $P6_3cm$. The positions of the Ba atoms were determined with the direct methods program SHELXS,[4] and the remaining atoms were located from analysis of difference electron density maps. Following refinement of the model with isotropic displacement coefficients on each atom, the data were corrected for absorption with the program DIFABS.[5] The heavy atoms (Ba and Sc) were refined with anisotropic displacement coefficients, the O atoms were refined with isotropic coefficients, and the B2 and B3 atoms were refined with isotropic coefficients constrained to that of the atom B1. The final cycle of full-matrix least-squares refinement with 1236 observed reflections having $F_o^2 > 3\sigma(F_o^2)$, 53

* To whom correspondence should be addressed.

⊗ Abstract published in *Advance ACS Abstracts*, October 15, 1994.

(1) Thompson, P. D.; Keszler, D. A. *Chem. Mater.*, previous paper in this issue.

(2) Thompson, P. D.; Huang, J.; Smith, R. W.; Keszler, D. A. *J. Solid State Chem.* **1991**, *95*, 126.

(3) Molecular Structure Corporation, TEXSAN, Single Crystal Structure Analysis Software, Version 5.0, 1980. MSC 3200 A Research Forest Drive, The Woodlands, TX 77381.

(4) Sheldrick, G. M. *Crystallographic Computing 3*; Sheldrick, G. M., Krüger, C., Goddard, R., Eds.; Oxford University Press: Oxford, 1985; p 175.

(5) Walker, N.; Stuart, D. *Acta Crystallogr., Sect. A* **1983**, *39*, 158.

0897-4756/94/2806-2008$04.50/0 © 1994 American Chemical Society

Table 1. Crystallographic Data and Experimental Conditions for $Ba_3Sc(BO_3)_3$

formula	$Ba_3Sc(BO_3)_3$
FW, amu	633.37
space group	$P6_3cm$ (No. 185)
a, Å	9.227(2)
c, Å	17.135(3)
V, Å^3	1277.2(5)
Z	6
T of data collection, K	293
ϱ_{calcd}, g cm^{-3}	4.940
radiation	graphite-monochromated Mo Kα (λ = 0.710 69 Å)
μ, cm^{-1}	144.9
transmission factors	0.76−1.00
$F(000)$	1656
$R_w(F_o)$	0.079
$R(F_o)$ for $F_o^2 > 3\sigma(F_o^2)$	0.057

Table 2. Atomic Parameters for $Ba_3Sc(BO_3)_3$[a]

atom	x	y	z	B_{eq}
Ba1	0	0	0	0.70(3)
Ba2	0.6774(1)	0	0.1535(2)	0.61(4)
Ba3	0.6571(1)	0	0.9041(2)	0.55(4)
Ba4	1/3	2/3	0.0515(1)	0.94(3)
Sc1	2/3	1/3	0.2795(4)	0.53(6)
Sc2	0	0	0.2843(4)	0.21(8)
O1	0.520(1)	0.662(1)	0.2045(6)	0.5(1)
O2	0.485(3)	0	0.0272(8)	1.0(3)
O3	0.196(1)	0	0.2149(8)	0.4(1)
O4	0.175(1)	0	−0.1391(8)	0.6(2)
O5	0.333(2)	0.148(2)	0.0280(6)	0.6(1)
O6	0.329(1)	−0.155(1)	−0.1515(8)	1.1(2)
B1	0.327(3)	0	0.034(2)	0.6(1)
B2	0.329(2)	0	−0.154(1)	0.6
B3	0.338(2)	0	0.202(1)	0.6

[a] $B_{eq} = 8(\pi^2/3)\Sigma_i\Sigma_j U_{ij}a^*_i a^*_j a_i a_j$.

parameters, and a secondary extinction coefficient = 1.20(8) × 10^{-6} converged to unweighted and weighted agreement factors of R = 0.057 and R_w = 0.079, respectively. The final electron density map revealed no peak greater than 2.4% of a Ba atom. Crystal data and final atomic parameters are listed in Tables 1 and 2, respectively.

Luminescence. Spectral data were obtained on a spectrometer assembled in this laboratory. For excitation of the Eu^{3+} samples, 392-nm light was selected with a Cary Model 15 prism monochromator from an Oriel 300 W Xe lamp. The emission wavelengths for all samples were scanned with an Oriel model 22500 1/8−m monochromator. The signal was detected with a Hamamatsu R636 photomultiplier tube, amplified with a Keithley Model 602 picoammeter, and digitized for computer acquisition and analysis. Spectrometer control software has been written in this laboratory.

Thermal Analysis. DTA scans were performed by using a Harrop Model DT-724 differential thermal analyzer and a Eurotherm Model 808 programmable temperature controller. This instrument is interfaced to an IBM PC/XT via a real-time device AD100A A/D converter and a Metrabyte M1351 signal conditioning module. Data acquisition software has been written in this laboratory. Samples and the alumina reference were enclosed in Pt cups and heated at 15 °C/min. Melting and decomposition temperatures were corrected by using the melting point of Au as a standard.

SHG Measurements. Optical second harmonic generation (SHG) measurements were performed on crystalline samples having particle sizes in the range 100−200 μm selected by using NIST standard sieves. A beam from a Molectron MY-34 series Q-switched Nd:YAG laser configured to operate at λ = 1064 nm was passed through a Corning 7−59 filter, to exclude 532-nm light, and onto the sample. A dichroic mirror was used to discriminate between the second harmonic (passed to detector) and the fundamental (reflected to a beam stop). The second harmonic was passed through a Corning 7-60 filter and detected with an RCA IP28A PMT.

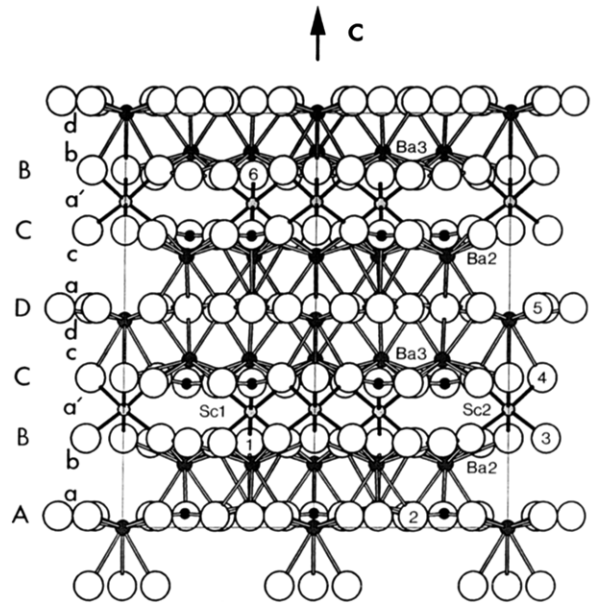

Figure 1. Drawing of the unit cell of $Ba_3Sc(BO_3)_3$ viewed along [110]. The large open circles represent O atoms, the small light shaded circles with dark bonds represent Sc atoms, the small dark shaded circles with open bonds represent Ba atoms, the dark-solid circles represent B atoms. Lettering along the left side corresponds to the layering sequence. Ba1 and Ba4 atoms are located in layers d and a, respectively. O atoms are labeled with numbers only.

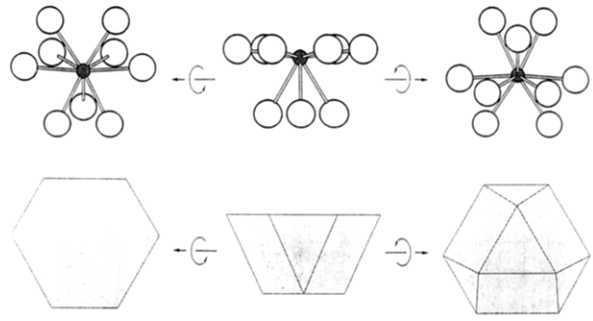

Figure 2. Sketch of the BaO_9 coordination environment with both ball-and-stick and polyhedral representations. All rotations are 90°.

Results and Discussion

Structure. The structure of $Ba_3Sc(BO_3)_3$ is a new type (Figure 1) containing discrete layers of triangular, planar BO_3 groups that stack orthogonal to the c axis. These layers are interleaved by planes of Ba and Sc atoms to give the overall stacking sequence AabBa′C-cdDacCa′BbdA, where the capital letters represent layers of BO_3 groups, the lower case letters represent layers of Ba atoms, and the lower case primed letters represent layers of Sc atoms. The two crystallographically independent types of Sc atoms occupy distorted octahedral sites having C_3 and C_{3v} point symmetries, and the four types of Ba atoms occupy nine-vertex polyhedra having distorted, parallel hexagonal, and trigonal bases. In this environment, each Ba atom binds six O atoms at the vertices of a distorted hexagon in one plane and three additional O atoms in a subjacent plane (Figure 2).

The Sc (a′) layers contain both crystallographic types of atoms sandwiched between arrays of BO_3 groups (BC). The distorted ScO_6 octahedra within each layer are isolated by the bridging BO_3 groups. These scan-

Table 3. Interatomic Distances (Å) and Angles (deg) for $Ba_3Sc(BO_3)_3$

Ba1−O4 × 3	2.88(1)	O5−Ba1−O5	66.1(5)
			51.8(5)
			158.4(4)
		O5−Ba1−O4	69.5(3)
Ba1−O5 × 6	2.72(2)	O4−Ba1−O4	58.3(4)
Ba1−O (avg)	2.77(8)		
Ba_2−O1 × 2	2.85(1)	O1−Ba2−O1	64.0(3)
			144.0(4)
Ba2−O1 × 2	2.88(1)	O1−Ba2−O3	47.7(3)
Ba2−O3 × 2	2.816(5)	O3−Ba2−O5	77.5(4)
Ba2−O5 × 2	2.72(1)	O5−Ba2−O5	66.1(6)
Ba2−O2	2.81(2)		
Ba2−O (avg)	2.82(6)		
Ba3−O4 × 2	2.852(4)	O6−Ba2−O6	62.2(4)
Ba3−O6 × 2	2.80(1)	O4−Ba3−O6	52.1(3)
			145.0(4)
Ba3−O6×2	2.82(2)	O6−Ba3−O2	76.7(5)
Ba3−O4 × 2	2.853(4)	O4−Ba3−O5	69.4(4)
Ba3−O2	2.65(2)	O2−Ba3−O5	66.1(4)
Ba3−O (avg)	2.81(6)		
Ba4−O1 × 3	3.15(1)	O2−Ba4−O5	65.8(4)
			52.7(4)
			161.4(4)
Ba4−O2 × 3	2.714(2)	O1−Ba4−O5	68.6(3)
Ba4−O5 × 3	2.72(2)	O1−Ba4−O1	57.6(3)
Ba4−O (avg.)	2.86(22)		
Sc1−O1 × 3	2.17(1)	O6−Sc1−O6	90.1(5)
Sc1−O6 × 3	2.06(1)	O6−Sc1−O1	90.7(5)
Sc1−O (avg)	2.12(6)	O1−Sc1−O1	88.7(4)
Sc2−O3 × 3	2.17(1)	O4−Sc2−O4	84.7(6)
Sc2−O4 × 3	2.09(1)	O4−Sc2−O3	91.1(3)
Sc2−O (avg)	2.13(4)	O3−Sc2−O3	92.8(5)
B1−O2	1.47(3)	O5−B1−O5	123.2(2.7)
B1−O5 × 2	1.35(2)	O2−B1−O5	117.6(1.2)
B1−O (avg)	1.39(7)		
B2−O4	1.45(2)	O6−B2−O6	119.9(1.6)
B2−O6 × 2	1.44(1)	O4−B2−O6	119.2(9)
B2−O(avg)	1.44(1)		
B3−O1 × 2	1.32(1)	O1−B3−O1	119.8(1.6)
B3−O3	1.33(2)	O1−B3−O3	119.2(8)
B3−O (avg)	1.32(1)		

dium borate sandwiches are completely separated by chemically distinct layers of BO_3 groups (A and D) and two sets of Ba double layers of the type a, b, c, and d (cf. Figure 1). The ScO_6 groups connect to the Ba atoms in two ways—each O···O edge in the trigonal faces of the distorted octahedron is common to a distorted hexagonal base of a Ba2−O_9 or Ba3−O_9 unit, and one trigonal face from each octahedron is common to a coordination environment of a Ba1 or Ba4 atom.

The four crystallographically dissimilar Ba atoms occupy sites with the following symmetries: Ba1, C_{3v}; Ba2, C_s; Ba3, C_s; Ba_4, C_3. Each Ba layer contains only one type of Ba atom, and within a layer the BaO_9 polyhedra have similar dispositions of their hexagonal and trigonal bases relative to the *c* axis (cf. Figure 1). This disposition reverses—the polyhedra are inverted—between adjacent planes within the four-layer Ba sequence (cdac ≡ Ba3·Ba1·Ba4·Ba2).

Selected interatomic distances and angles are listed in Table 3. The range of Sc−O distances 2.06(1) to 2.17(1) Å is similar to that found in $Sr_3Sc(BO_3)_3$, 2.077(2) and 2.142(2) Å.[1] Additional distortions of the ScO_6 environments from O_h symmetry are indicated by the O−Sc−O angles that extend from 84.7(6) to 92.8(5)°. These distortions are related to the displacement of the Sc atom from the medial plane between the trigonal faces of the octahedra. The displacements arise in part from the anisotropic connectivity of the trigonal faces to the Ba-centered polyhedra; only one trigonal face of each octahedron is shared with a Ba atom.

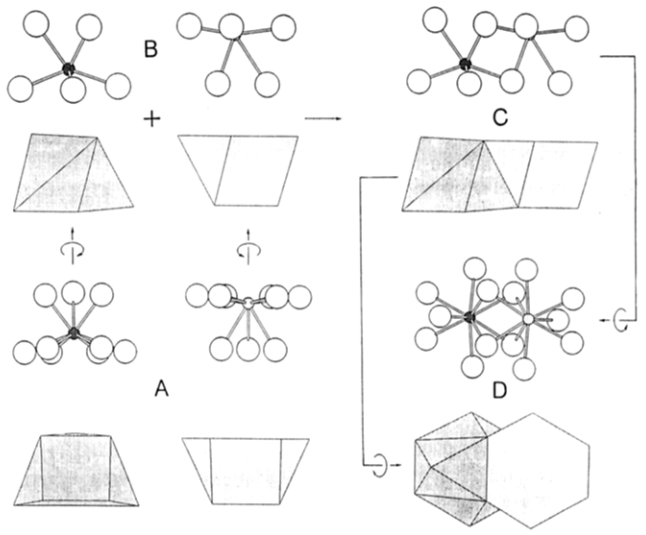

Figure 3. Illustration of rectangular face sharing between BaO_9 coordination environments. Both ball-and-stick and polyhedra representations are shown. (A) Environments oriented to easily view rectangular faces. (B) Rotation by 90° to align rectangular faces (as in structure). (C) BaO_9 coordination environments sharing rectangular faces. (D) Rotation of 90° to view face sharing down *c* axis [001]. Note: A, B, and C are views perpendicular to *c* and D is coaxial with *c*.

The polyhedra centered by atoms Ba3 and Ba1, and Ba4 and Ba2 share rectangular faces defined by two O atoms from the 6-fold base and two O atoms from the triangular base (Figure 3). Face sharing also occurs via the triangular bases of the polyhedra centered by atoms Ba2 and Ba3. All face sharing occurs between two different Ba layers.

Distances for the Ba−O interactions range from 2.65(2) to 3.15(1) Å with the average being 2.8(1) Å. Several O−Ba−O angles are of interest—those in the 6-fold base, those in the triangular base, and those between the two bases. In general, the distortion in the 6-fold base is the result of two different angles that alternate around the hexagon. There is a small angle in the range $46.8(3) < \theta < 52.7(4)°$ and a larger one in the range $59.0(5) < \theta < 69.4(4)°$. The smaller angles are constrained by edge sharing with BO_3 groups, and the larger angles are associated by edge sharing with the ScO_6 groups. The average O−Ba−O angle in the triangular bases is 63(4)° and the average O−Ba−O angle between the two bases is 72(4)°.

The BaO_9 polyhedron is similar to that of KO_9 in the compound buetschliite, $K_2Ca(CO_3)_2$.[6] Similar small O−K−O angles in the 6-fold base are constrained by CO_3 groups. Atom Ba1 in the title structure and atom K in buetschliite both occupy sites having C_{3v} point symmetry. Distances in the 6-fold base are 2.72(2) Å for Ba1−O and 2.80 Å for K−O, and distances in the trigonal base are 2.88 Å for Ba1−O and 3.01 Å for K−O. As viewed along the *c* axis, atom Ba1 is displaced 0.36 Å from the 6-fold base and 2.38 Å from the trigonal base. In buetschliite, the K atom is displaced 0.72 Å from the 6-fold base and 2.45 Å from the trigonal base.

The BO_3 units have C_s symmetry. The average B−O bond distance of 1.39(6) Å compares well to the average distance of 1.38(1) Å found in $Sr_3Sc(BO_3)_3$.[1] O−B−O angles range from 117.6(1.2) to 123.2(2.7)° with the average being 119.4(1.6)°.

(6) Pabst, A. *Am. Mineral.* **1974**, 353.

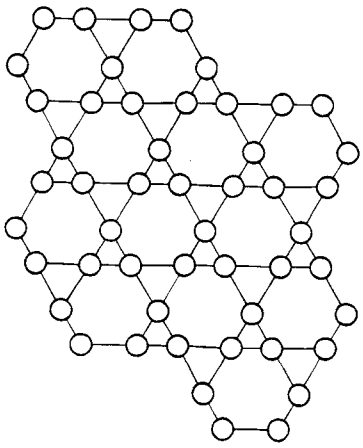

Figure 4. Layer of O atoms orthogonal to the *c* axis forming a semiregular four-connected net consisting of distorted hexagons and two different sizes of triangles.

Six O atoms are distributed through two types of symmetry sites. Atoms O1, O5, and O6 occupy general positions, while atoms O2, O3, and O4 reside in sites having C_s point symmetry. Atoms O3 and O6 have a coordination number of 4 and occupy highly distorted tetrahedra, while atoms O1, O2, O4, and O5 have a coordination number of 5. Because the compound is a simple orthoborate, each O atom is bound to only one B atom. The remaining connectivities between the O atoms and the metal atoms may be discerned by inspection of Table 3. Each layer of O atoms extending orthogonal to the *c* axis may be described as a semiregular net consisting of triangles and hexagons. A similar network has been described by Wells.[7] The net characterized by Wells has uniform triangles and hexagons while the nets formed in $Ba_3Sc(BO_3)_3$ consist of distorted hexagons and two different sizes of triangles (Figure 4). The smaller triangles are occupied by B atoms to form the BO_3 units and the larger triangles are defined as trigonal faces of the ScO_6 octahedra or triangular faces of the BaO_9 polyhedra or both. Examination of the polygons discloses the identity of the net as being four connected (each polygon comes to an intersection with three others). The general equation for a four connected net is $3\phi_3 + 4\phi_4 + 5\phi_5 + 6\phi_6 + 7\phi_7 + 8\phi_8 + ... + n\phi_n = 4$, where ϕ_n = fraction of polygons in the net and n = the number of sides on a polygon. Since the net in $Ba_3Sc(BO_3)_3$ consists of triangles and hexagons, the equation reduces to $3\phi_3 + 6\phi_6 = 4$. Therefore, two-thirds of the polygons in the net are triangles, ϕ_3, and one-third are hexagons, ϕ_6.

Structure Field. To aid in establishing the limits of the structure field, the existence of the compounds $Ba_3Ln(BO_3)_3$ (Ln = lanthanide) was determined, and the solid-solution series $Ba_3Y_{1-x}Eu_x(BO_3)_3$, ($0 \le x \le 0.5$) was examined.

In the series $Ba_3Ln(BO_3)_3$, the $Ba_3Sc(BO_3)_3$ structure type forms for Ln = Dy, Ho, Y, Er, Tm, Yb, Lu, and Sc. Formulations containing an Ln atom with a crystal radius larger than that of Dy or another atom with a radius smaller than that of Sc do not produce the title structure under the high-temperature synthetic conditions described in the experimental section. A plot of unit cell volume vs the radius of the M^{3+} cation (Figure 5) exhibits the expected trend of increasing unit-cell volume with increasing crystal radius.

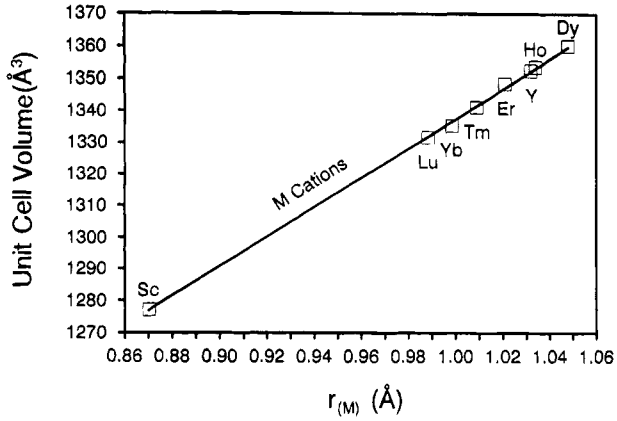

Figure 5. Plot of unit-cell volume of $Ba_3M(BO_3)_3$ compounds versus M^{3+} cation radius.

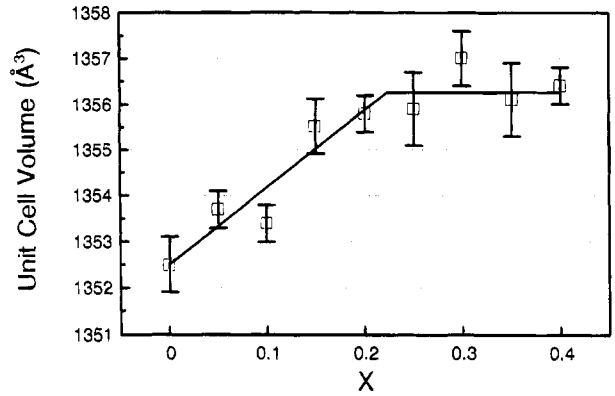

Figure 6. Plot of unit-cell volume for the compounds $Ba_3Y_{1-x}Eu_x(BO_3)_3$ versus mole fraction of Eu^{3+}, x. Error bars are 2σ in each case.

The compound $Ba_3In(BO_3)_3$ represents an anomaly in this study.[8] The radius of In^{3+}, 0.940 Å, is between those of Lu^{3+}, 1.001 Å , and Sc^{3+}, 0.885 Å ,easily placing the compound within the structure field. We have found, however, that the material crystallizes only in the structure type of $Sr_3Sc(BO_3)_3$.[9,10] This behavior is discussed in more detail in the next paper of this series.

An additional method for determining the maximum crystal radius of the Ln atom that leads to stabilization of the structure is provided by the series $Ba_3Y_{1-x}Eu_x(BO_3)_3$. By plotting unit cell volume vs the mole fraction of Eu^{3+} (Figure 6), the solubility of Eu^{3+} in the structure may be determined. The hypothetical compound $Ba_3Eu(BO_3)_3$ is outside the structure field and does not form. By substituting Eu^{3+} for Y^{3+}, a steady increase in unit cell volume occurs up to $x \approx 0.2$. For larger values of x, the unit-cell volume remains constant, so $x \approx 0.2$ represents an approximate solubility limit. The volume change over the entire range of x is less than 5 Å^3. Such a small change in unit-cell volume makes it difficult to choose with precision the limit of Eu^{3+} solubility from the X-ray data alone. The value $x \approx 0.2$, however, is also supported by the spectral data

(7) Wells, A. F. *Structural Inorganic Chemistry,* 5th ed.; Oxford University Press: Oxford, 1984.

(8) Schaffers, K. I. Ph.D. Dissertation, Oregon State University, 1992. Cox, J. R. Ph.D. Dissertation, Oregon State University, 1994.

(9) Schaffers, K. I.; Alekel, T., III; Thompson, P. D.; Cox, J. R.; Keszler, D. A. *J. Am. Chem. Soc.* **1990**, *112*, 7068.

(10) Schaffers, K. I.; Thompson, P. D.; Alekel, T., III; Cox, J. R.; Keszler, D. A. *Chem. Mater.*, following paper in this issue.

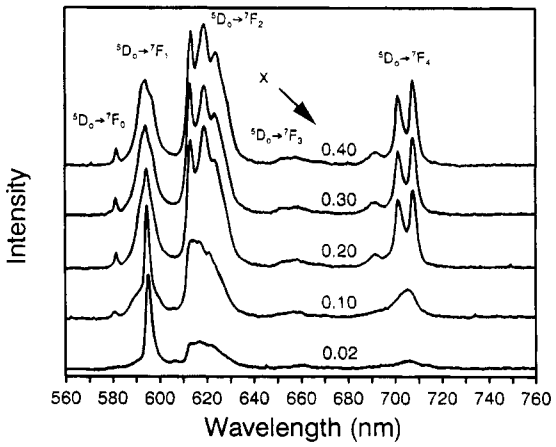

Figure 7. Emission spectra of samples from the series $Ba_3Y_{1-x}Eu_x(BO_3)_3$ with peaks labeled according to the assigned transitions.

that are discussed below. This value of x corresponds to an effective radius for the M cation of 1.050 Å, which compares well to the radius of Dy^{3+} = 1.052 Å,[11] the largest M atom that has been stoichiometrically incorporated into the structure. (The effective M radius was calculated as the weighted average of the Eu^{3+} and Y^{3+} crystal radii: $R_{eff} = (0.2)(R_{Eu}) + (0.8)(R_Y) = (0.2)(1.087$ Å$) + (0.8)(1.040$ Å$) = 1.050$ Å.)

Emission spectra were also recorded on this series of Y–Eu samples. These data yield information concerning the site preference of the dopant Eu^{3+} ion within the crystal structure as a function of concentration. Elucidation of this preference was accomplished by examination of the peaks in the emission spectrum associated with the electric-, $^5D_0 \rightarrow {}^7F_2$, $^5D_0 \rightarrow {}^7F_4$, and magnetic-dipole, $^5D_0 \rightarrow {}^7F_1$, allowed transitions.[12] If the Eu^{3+} ion occupies a site having a center of symmetry, electric-dipole transitions are forbidden while magnetic-dipole transitions are weakly allowed through spin–orbit coupling. If the ion inhabits a site without a center of symmetry, odd crystal field terms contribute to the allowed nature of the electric- and magnetic-dipole transitions. In this case, however, the magnetic-dipole transitions are much less intense than the electric-dipole transitions and may appear to be absent.

In the compounds $Ba_3Y_{1-x}Eu_x(BO_3)_3$, the Ba atoms occupy noncentrosymmetric sites and the Y atoms nearly centrosymmetric sites. The spectrum for x = 0.02 indicates that Eu^{3+} substitutes onto the Y site since the peaks representing magnetic-dipole allowed transitions are dominant. The peaks in this spectrum representing electric-dipole transitions, though very weak in intensity, likely result from the *nearly* centrosymmetric Y site not having an actual inversion center. As x increases to 0.2, peaks representing the electric-dipole transitions heighten in intensity. These data indicate that the Eu^{3+} ion prefers the 6-fold M site at low concentrations. For larger values of x, the ion appears to be distributed over both the M and Ba sites with an increasing occupation of the Ba sites at higher concentrations (Figure 7).

Again, the compound *$Ba_3Eu(BO_3)_3$* does not form, implying that there is a limit to the solubility of Eu^{3+} in the structure. When that limit is reached and

(11) Shannon, R. D. *Acta Chystallogr., Sect. A* **1976**, *32*, 751.
(12) Blasse, G.; Bril, A. *Philos. Technol. Rev.* **1970**, *31*, 303.

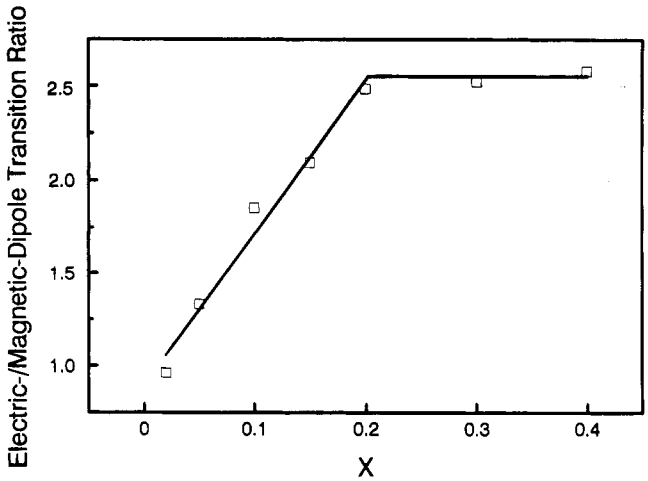

Figure 8. Plot of peak area ratio for electric- and magnetic-dipole allowed transitions ($^5D_0 \rightarrow {}^7F_2/{}^5D_0 \rightarrow {}^7F_1$) versus composition ($x$) of Eu^{3+} in the compounds $Ba_3Y_{1-x}Eu_x(BO_3)_3$.

Table 4. Decomposition, Phase Change, and Melting Temperatures (°C) for $Ba_3M(BO_3)_3$ Compounds

compound	phase change/decomposition	melting
$Ba_3Sc(BO_3)_3$		1200
$Ba_3Lu(BO_3)_3$		1257
$Ba_3Yb(BO_3)_3$		1216
$Ba_3Tm(BO_3)_3$		1218
$Ba_3Er(BO_3)_3$	1173[a]	1239
$Ba_3Y(BO_3)_3$	1148[a]	1265
$Ba_3Ho(BO_3)_3$	1127[a]	1229
$Ba_3Dy(BO_3)_3$	953[b]	1237

[a] Temperature of a phase transformation. [b] Temperature of a decomposition.

exceeded, at $x \geq 0.2$, the resulting spectra become similar (samples with x = 0.20, 0.30, and 0.40). From X-ray data, we have found that the samples with x > 0.20 have the same structural compositions - they are mixtures of $Ba_3Y_{0.80}Eu_{0.20}(BO_3)_3$ and amorphous materials. It is unlikely that Eu^{3+} occupies a centrosymmetric site within the amorphous phase(s). Luminescence originating here would, therefore, add to the peaks representing electric-dipole allowed transitions. The relative magnitudes of the electric- and magnetic-dipole peaks, however, remain essentially constant for $x > 0.2$, so the contribution of the amorphous materials to the luminescence is assumed to be negligible under these excitation conditions. Not only are these data consistent with the solubility limit of Eu^{3+} as determined from the X-ray data, but also they reveal the distribution of Eu^{3+} ions over the crystallographic sites within the structure.

To further substantiate the X-ray data, ratios of peak areas for the electric- ($^5D_0 \rightarrow {}^7F_2$) and magnetic- ($^5D_0 \rightarrow {}^7F_1$) dipole transitions have been plotted against the mole fraction of Eu^{3+}, x (Figure 8). The break in the line near x = 0.2 is again consistent with the results derived from X-ray data.

DTA. Thermal analysis data were obtained for each compound (Table 4). Peaks representing two thermal events were observed in the heating curves for compounds with M = Dy, Ho, Y, and Er. The peaks at the higher temperatures correspond to melting, and the signals at the lower temperatures have been found to correspond to peritectic reactions or phase transformations. The nature of the transformations was determined by annealing samples at temperatures intermediate to those of the two thermal events. Analysis of

the X-ray patterns from the resulting powders indicates that the compound $Ba_3Dy(BO_3)_3$ decomposes to form $Ba_3Dy_2(BO_3)_4$ + $Ba_3(BO_3)_2$, while the Ho, Y, and Er derivatives retain their stoichiometries and undergo a structural phase change from the layered arrangement of $BaSc_3(BO_3)_3$ to the three-dimensional STACK[9,10] structure of $Sr_3Sc(BO_3)_3$. The Tm, Yb, Lu, and Sc compounds yield only peaks representing melting events, an indication that these compounds may melt congruently. These data are consistent with a greater structural stability for the Sc and smaller lanthanide derivatives. In particular, the temperature of the phase transformation or decomposition decreases systematically with an increase in the size of the lanthanide atom.

Optical Second-Harmonic Generation. Because the structure type is noncentrosymmetric, a Kurtz–Perry optical second-harmonic test[13] was performed on a microcrystalline sample of $Ba_3Sc(BO_3)_3$. A small signal corresponding to <0.1 times the value of quartz was observed. This result is completely consistent with the structure. It is well established that the principal chromophores in this type of material are the nonequivalent BO_3 groups.[8,14] A simple examination of the distribution of these groups in the structure reveals that they are related by an approximate center of symmetry. This leads to a net cancellation of the microscopic hyperpolarizability coefficients and the small observed macroscopic nonlinearity. Indeed, the noncentrosymmetric character of the structure is primarily dictated by the distribution of the Ba atoms.

Acknowledgment. This work was supported by the U.S. National Science Foundation, Solid State Chemistry Program. Acknowledgment is made to the donors of The Petroleum Research Fund, administered by the American Chemical Society, for partial support of the research. D.A.K. thanks the Alfred P. Sloan Foundation for a fellowship.

Supplementary Material Available: Listings of anisotropic displacement coefficients and complete crystal and structure solution data (2 pages). Ordering information is given on any current masthead page.

(13) Kurtz, S. K.; Perry, T. T. *J. Appl. Phys.* **1968**, *39*, 3798.

(14) Chen, C.; Wu, Y.; Li, R. *J. Cryst. Growth* **1990**, *99*, 790.